Pure and Applied Geophysics

Neotectonics at the SE Continental Margin of the Korean Peninsula: Implications for the Back-Arc Region Behind the SW Japan Arc

HAN-JOON KIM,[1] SEONGHOON MOON,[1] CHUNGHO KIM,[1] KWANG-HEE KIM,[2] WOOSEOK SEO,[2] KWANG-HYUN CHO,[3] HYE-JIN MOON,[1] and GWANG HOON LEE[4]

Abstract—The geological evolution of the SE continental margin of the Korean Peninsula resulted from crustal extension with back-arc rifting to spreading (from the Late Oligocene to the Middle Miocene) and crustal shortening with back-arc closing (from the Middle Miocene to the present), associated with the separation of the SW Japan Arc. Earthquakes occur more frequently in this region compared to other offshore regions of the Korean Peninsula; among them, the M_w 5.0 earthquake that occurred in 2016 is the largest event ever recorded instrumentally. We investigate the geological structure of the epicentral area of the M_w 5.0 earthquake and address neotectonic activity at the margin. Seismic reflection profiles reveal abundant faults in the epicentral area that make up strike-slip fault systems. A fault system encompassing the epicenter of the M_w 5.0 earthquake is suggested as the source structure, with its attitude consistent with the focal mechanism solution. We propose that the M_w 5.0 earthquake occurred due to the reactivation of an extensional fault created during back-arc rifting which currently induces dextral slip under the ENE–WSW-oriented compressional stress field in and around the Korean Peninsula. The maximum magnitude of earthquakes expected at the margin is estimated as no higher than M_w 6.0. Restoration of seismic profiles indicates that the current stress field was established after 5.5 Ma. The S-wave velocity structure of the uppermost mantle shows asthenospheric upwelling elongated along the continental margin, which may be considered an important regional source of the current stress field by inducing convection in the uppermost mantle toward the Korean Peninsula lithosphere.

Keywords: Continental margin of the Korean Peninsula, neotectonics, seismic profiles, fault mapping, cross-section restoration, stress field.

[1] Marine Active Fault Research Group, Korea Institute of Ocean Science and Technology, Busan 49111, Republic of Korea. E-mail: hanjkim@kiost.ac.kr
[2] Department of Geological Sciences, Pusan National University, Busan 46241, Republic of Korea.
[3] Domestic Business Department, Korea National Oil Corporation, Ulsan 44538, Republic of Korea.
[4] Department of Energy Resources Engineering, Pukyong National University, Busan 48513, Republic of Korea.

1. Introduction

Back-arc rifting to spreading behind the Japan Arc in the NW Pacific subduction zone commenced in the Late Oligocene, separating the SW Japan Arc from (near) the SE Korean Peninsula. As a result, the crustal structure and nature vary across the continental margin of the Korean Peninsula from rifted continental crust under the continental shelf and the slope to back-arc oceanic crust under the Ulleung Basin (Fig. 1) (Kim et al., 2003, 2015). The continental margin encompassing the shelf and the slope is also characterized by the frequent occurrence of earthquakes that appear to delineate a zone of concentrated seismicity distinguished from the deep-seated Ulleung Basin with rare seismicity (Fig. 1b).

An earthquake with a moment magnitude (M_w) of 5.0 occurred at the SE continental margin of the Korean Peninsula on July 5, 2016 (Fig. 1b), herein referred to as the 2016 M_w 5.0 earthquake. The magnitude is exceptional because earthquakes in the area had been significantly less than 5.0 since the beginning of instrumental recording in 1978 in Korea. Although a large volume of multichannel seismic (MCS) profiles was acquired at the margin, faults or fault systems have not been identified in the epicentral area of the 2016 M_w 5.0 earthquake that can explain the focal mechanism. In addition, the relationship between crustal structure and seismicity, not directly related to plate boundary processes as in the trench zone off the Japan Arc, remains unknown.
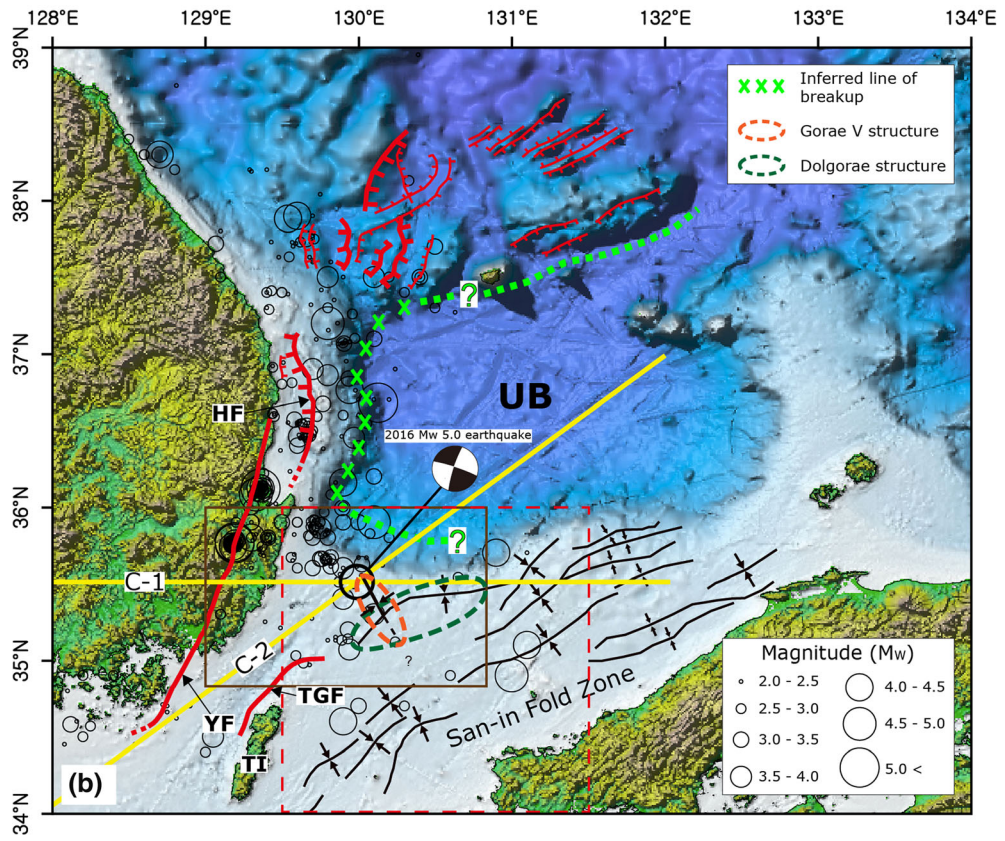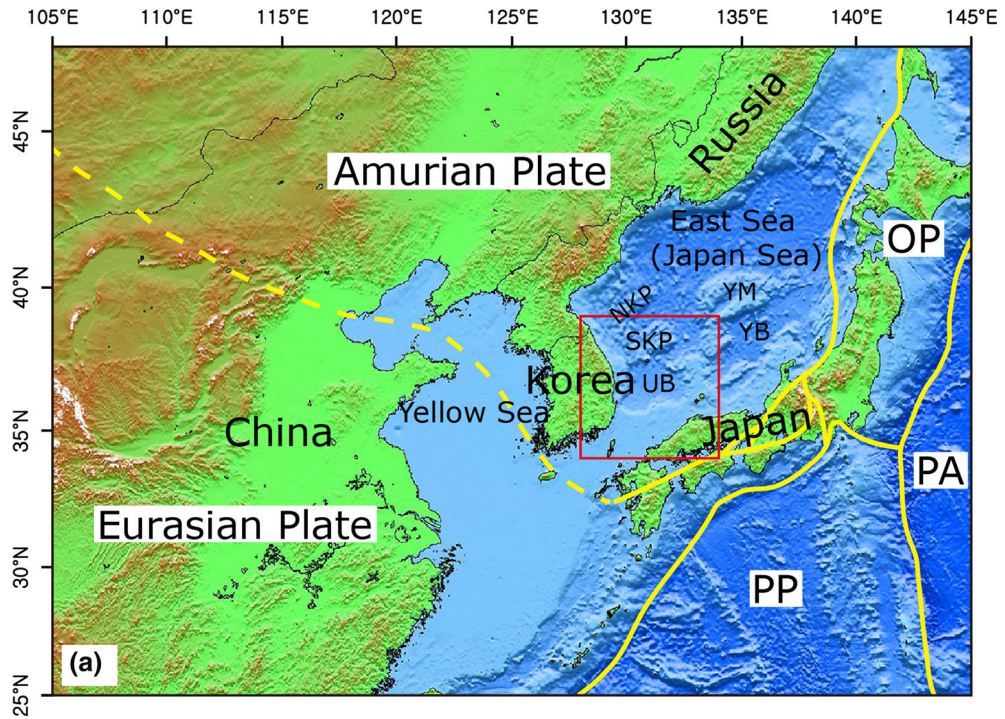
The objectives of this study are to correlate the 2016 M_w 5.0 earthquake with the geological structure and address the neotectonic activity at the SE continental margin of the Korean Peninsula. We first infer

◄Figure 1

a Plate boundaries in NE Asia (modified Taira, 2001). The red rectangle indicates the area in **b**. OP, PA, PP = Okhotsk Sea, Pacific, and Philippine Sea Plates, respectively. JB, UB, and YB = Japan, Ulleung, and Yamato Basins, respectively; NKP and SKP = North and South Korea Plateaus; YM = Yamato Bank. **b** Identified faults associated with back-arc rifting and the inferred locus of breakup at the continental margin of the Korean Peninsula (modified from Kim et al., 2008; Kim, Jou, et al., 2018). The focal mechanism solution of the 2016 M_w 5.0 earthquake is shown. C-1 and C-2 are two transects showing the V_s structure down to 50 km in Fig. 4. The epicenters and magnitude of earthquakes at the continental margin of the Korean Peninsula since 1978 are shown. The black rectangle indicates the area in Fig. 3 showing the locations of seismic profiles. The red dotted-line rectangle indicates the area for statistically computing the maximum expected magnitude of earthquakes. HF, YF, and TGF = Hupo, Yangsan, and Tsushima-Goto Faults; TI = Tsushima Island)

the tectonic structure below the epicentral area from available P-wave crustal velocity models from deep seismic sounding (Cho et al., 2006; Kim et al., 2003) and the S-wave velocity (V_s) model of NE Asia down to the uppermost mantle from ambient noise tomography (Zheng et al., 2011). We then identify faults in the epicentral area on prolific MCS profiles obtained so far and assess the consistency between the fault geometry and the focal mechanism of the 2016 M_w 5.0 earthquake. Additionally, the maximum expected magnitude of earthquakes (M_{max}) in the epicentral area is estimated using the area-specific stochastic method described by Kijko et al. (2016). We also restore sequentially two seismic profiles crossing the epicentral area to understand its geological evolution. Finally, we infer the origin of the current stress field responsible for the neotectonic activity at the continental margin of the Korean Peninsula.

2. Tectonic Setting

Back-arc opening in the NW Pacific subduction zone separated the Japan Arc from NE Asia in Late Oligocene through Middle Miocene times (Fig. 2). The SW Japan Arc migrated away from (near) the Korean Peninsula (Kim et al., 2015 and references therein) emplacing the present SE continental margin of the Korean Peninsula that comprises the continental shelf and slope region descending to the floor

of the Ulleung Basin. Studies on the crustal structure and rift architecture at the continental margin of the Korean Peninsula (Kim et al., 2007, 2015) and on paleomagnetic signals (Hoshi, 2018; Vaes et al., 2019; van Horne et al., 2017 and references therein) suggest that (1) back-arc rifting commenced in the Late Oligocene and gave way to back-arc spreading, with a significant amount of clockwise rotation of the SW Japan Arc that culminated in the Early Miocene (Fig. 2a, c), and (2) the SE continental shelf and the slope of the Korean Peninsula are the region of rifted continental crust, whereas the Ulleung Basin is underlain by back-arc oceanic crust that is thicker than normal oceanic crust by 2–3 km. This is consistent with studies on age dating and geological correlation between the peninsula and the arc (Hisada et al., 2008; Kojima et al., 2008; Takahashi et al., 2018).

We note that an alternative explanation for the separation of the Japan Arc from NE Asia is a southward translation of the arc between two major N–S strike-slip zones oriented approximately N–S (e.g., Jolivet et al., 1994) combined with clockwise rotation of the SW Japan Arc (Jolivet et al., 1995). This model suggests that the western fault zone extends from the Tsushima-Goto Fault (Fig. 1b) (Jolivet et al., 1994) to the north along the continental slope of the Korean Peninsula (Yoon & Chough, 1995); the eastern fault zone extends across the NE Japan Arc (Jolivet et al., 1994).

Earlier than the Middle Miocene, large-scale plate reorganization took place in East Asia, which caused the Philippine Sea Plate to move northward and collide with the SW Japan Arc (Fig. 2d) (e.g., Hall et al., 1995; Sibuet et al., 2002). The collision induced tectonic switching from back-arc opening to back-arc closing behind the Japan Arc (Lee et al., 2011). As a result, NNW–SSE (or NW–SE) compression deformed the continental shelf between the Korean Peninsula and the SW Japan Arc from ∼ 15 Ma, forming a series of ENE–WSW (or NE–SW)-trending thrusts and anticlines including the Dolgorae structure and the San-in Fold Zone (or Taiwan-Shinji Fold Zone) (Fig. 1b) (Kim et al., 2008; Kimura et al., 2005). Later, possibly in the Early Pliocene after 5.5 Ma, the direction of compression changed to ENE–WSW (or E–W) that has persisted

Figure 2
Schematic diagrams showing the processes of back-arc evolution associated with the separation of the Japan Arc from the Korean continental margin (modified from Kim, Jou, et al., 2018). **a** Initiation of back-arc rifting and breakup behind the Japan Arc. **b** Back-arc rifting and breakup at the eastern Korean margin. **c** Back-arc spreading and clockwise rotation of the SW Japan Arc. **d** Back-arc closing

to the present in and around the Korean Peninsula and that created a NNW–SSE-trending small anticline, the Gorae V structure, on the SE continental shelf of the peninsula (Lee et al., 2011). The 2016 M_w 5.0 earthquake occurred in the northern edge of the Gorae V structure (Fig. 1b). Lee et al. (2011) attributed the change in the direction of compression to the eastward movement of the Amurian Plate that was fragmented from the Eurasian Plate in the Pliocene as a microplate and has been moving eastward or east-

northeastward relative to the Eurasian Plate. The Amurian Plate includes NE China, the Korean Peninsula, Russian Far East, and the SW Japan Arc (Fig. 1a) (e.g., Petit & Fournier, 2005). Kim, Yoon, et al. (2018) suggested incipient subduction of the back-arc oceanic crust underlying the Ulleung Basin at the continental margin of the Korean Peninsula since the Early Pliocene.

The continental shelf and slope region of the Korean Peninsula shows frequent seismicity; in

contrast, the Ulleung Basin underlain by back-arc oceanic crust has rare seismicity (Fig. 1b). This contrasting pattern may demarcate the rifted (i.e., highly faulted) continental and much less faulted back-arc oceanic crust. The epicenters of the earthquakes at the continental margin show a close spatial correlation with the structures resulting from back-arc rifting and breakup (Fig. 1b) (Kim, Jou, et al., 2018). The focal mechanisms at the Korean margin indicate dominantly either reverse or strike-slip motion or a combination of both with diverse fault strikes (Choi et al., 2012). Kim, Jou, et al. (2018) suggested that the changing geometry of rift faults and the breakup locus following a curvilinear path induces these focal mechanisms under the present ENE–WSW-trending compressional stress field.

3. Data

For mapping faults in the epicentral area of the 2016 M_w 5.0 earthquake, we use MCS profiles from 2-D and 3-D seismic data obtained using an air gun array as a source (Fig. 3). Profiles from 2-D data consist of (1) approximately 3400 km of migrated profiles from the Korea National Oil Corporation (KNOC), (2) 1700 km of stacked profiles from the Korea Institute of Geosciences and Minerals (KIGAM), and (3) 1100 km of migrated profiles from the Korea Institute of Ocean Science and Technology (KIOST). 3-D seismic data were obtained by the KNOC in a 36×27 km^2 area that includes the epicenter of the 2016 M_w 5.0 earthquake. 3-D data processing included 3-D prestack time migration.

Additionally, we obtained a set of high-resolution seismic data to image shallow structures using a sparker and a 24-channel streamer as a source and a receiver, respectively (Fig. 3). The streamer with a group interval of 6.25 m provided five- or sixfold coverage. A conventional data processing scheme was applied to this data set that included trace editing, muting, velocity analysis, and stack. For velocity analysis, the constant velocity stack (CVS) was applied because P-wave velocities (V_p) in sedimentary layers are not accurately determined using a

conventional velocity analysis method due to the short length (150 m) of the active section of the streamer.

The earthquake data used for stochastic estimation of M_{max} consist of the events recorded from March 1, 1982, to September 30, 2021, by the Korea Meteorological Administration (KMA), covering the area from 34.8° N to 36.0° N and from 129.0° E to 131.0° E. Out of the total events in the record, 175 offshore events were included in the catalog for estimating M_{max} that are larger than M_L 1.0 as a threshold magnitude for computation.

4. Focal Mechanism Solution of the 2016 M_w 5.0 Earthquake

The focal depth of the 2016 M_w 5.0 earthquake is 16 km, which is considerably deeper than the focal depths of the earthquakes in the Korean Peninsula, averaging about 10 km (Sheen, 2015). We used the HASH program (Hardebeck & Shearer, 2003) to determine the focal mechanism solution of the 2016 M_w 5.0 earthquake from P-wave first motions and S/P-wave amplitude ratios. The program is known to provide the most likely mechanism given an imperfect understanding of the seismic velocity structure, the event location, the polarity measurements, and other factors (Kilb & Hardebeck, 2006). We used polarity and S/P ratio data from Hi-net and F-net (Obara et al., 2005; Okada et al., 2004) and from the KMA. The earthquake was azimuthally well covered, which ensured a reliable focal mechanism solution. The result indicates a strike-slip focal mechanism; the fault movement was either right-lateral on a vertical NNE–SSW-striking fault with strike = 198°, dip = 84°, and rake = 174,° or left-lateral on a vertical WNW–ESE-striking fault with strike = 288°, dip = 84°, and rake = 6°. The solution also shows that the event has a compressional axis of stress (P-axis) in the ENE–WSW direction, which is consistent with those suggested in previous studies in the Korea Peninsula and its vicinity (e.g., Jun, 1991; Kim & Park, 2010; Rhie & Kim, 2010).
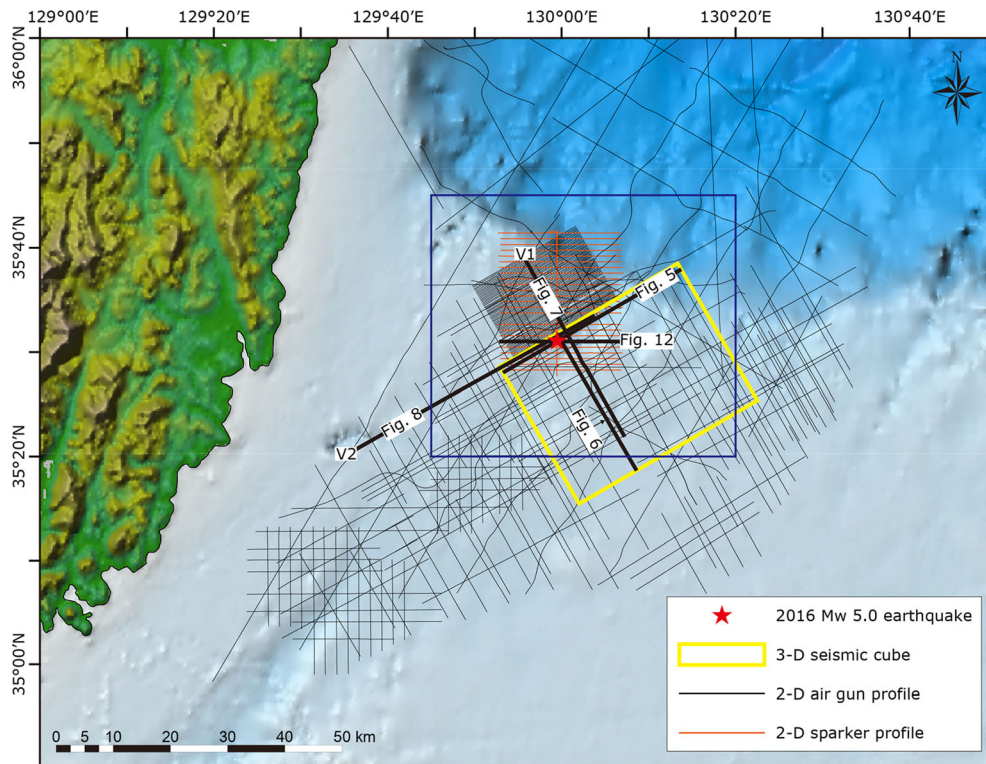
Figure 3
Locations of seismic profiles. The seismic profiles referred to in the text are highlighted as thick lines and labeled with a figure number. The yellow rectangle denotes the area of 3-D seismic data acquisition. The blue rectangle indicates the area showing fault traces in Fig. 9

5. Crustal Structure of the Continental Margin and Seismicity

Deep seismic sounding constrained the crustal V_p structure of the Korean Peninsula (Cho et al., 2006) and its continental margin into the Ulleung Basin (Kim et al., 2003). The Moho discontinuity below the SE part of the Korean Peninsula occurs at a depth slightly less than 30 km (Cho et al., 2006), whereas the Moho occurs at 16 km depth under the back-arc oceanic crust in the Ulleung Basin (Kim et al., 2003).

The 3-D crustal V_s structure of the Korean Peninsula and its margin is available from ambient noise tomography (Zheng et al., 2011). Figure 4 shows the crustal V_s structure along two lines, C-1 and C-2 in Fig. 1b, passing through the epicenter of the 2016 M_w 5.0 earthquake: (1) line C-1 from the southern Korean Peninsula through the SE margin toward the SW Japan Arc and (2) line C-2 from the SE continental shelf of the peninsula to the Ulleung

Basin. Comparing these V_s structures with the V_p structures in Kim et al. (2003) and Cho et al. (2006), we recognize that (1) the Moho depth under the Korean Peninsula is represented by the V_s contour of 4.0 km/s, (2) the boundary between the upper and lower continental crust follows approximately the V_s contour of 3.6 km/s, (3) the 2016 M_w 5.0 earthquake occurred in the lower part of the upper continental crust immediately above the upper/lower crustal boundary, and (4) the Moho depth under the Ulleung Basin correlates fairly well with V_s of 3.75 km/s, which is significantly lower than that under the Korean Peninsula. The back-arc oceanic crust under the Ulleung Basin was created above the hotter-than-normal mantle in relatively recent Late Oligocene to Early Miocene times (Kim et al., 2003), being currently characterized by heat flow exceeding 100 mW/m^2 (Horozal et al., 2009), which is much higher than that in the Korean Peninsula (Kim et al., 2015). The V_s is known to decrease significantly in a hot and
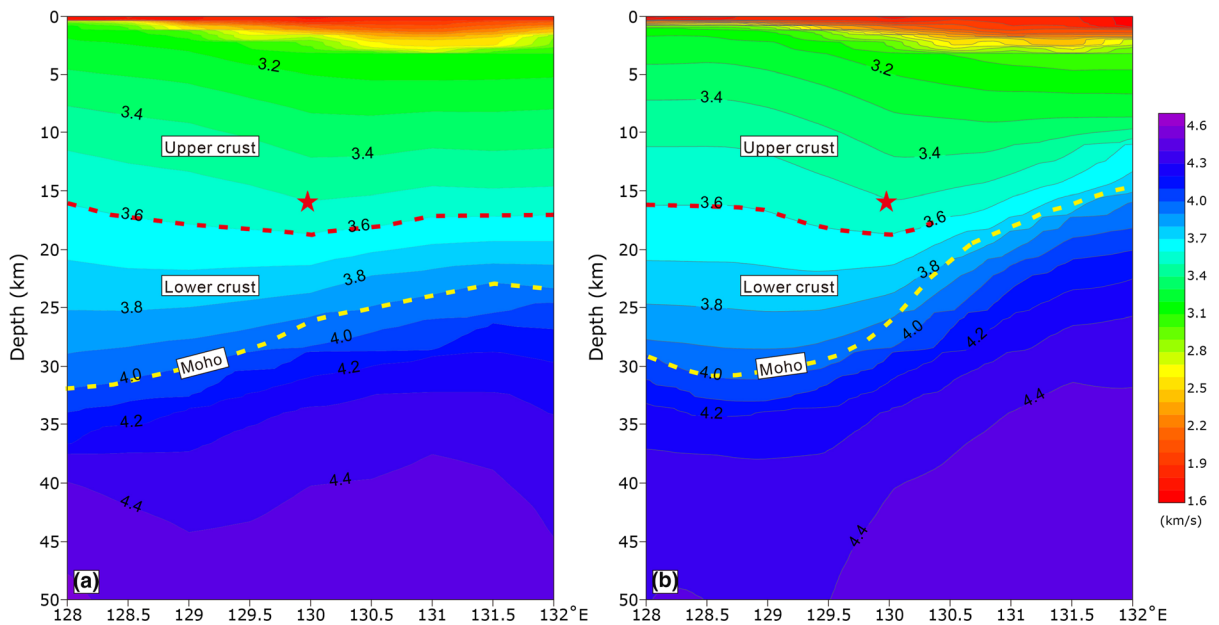
Figure 4

Vertical profiles showing V_s structure along **a** C-1 and **b** C-2 (see Fig. 1b for location). The Moho (yellow line) is estimated to be represented by the 4.0 km/s contour in the Korean Peninsula and the 3.75 km/s contour under the back-arc oceanic crust. The upper and lower crust boundary in continental crust is denoted by the red line. The red star denotes the hypocenter of the 2016 M_w 5.0 earthquake. The profiles were obtained by interpolation of the 3-D V_s structure in Zheng et al. (2011)

ductile medium (e.g., Carcione & Poletto, 2013), which probably explains the lower V_s at the Moho level under the hot and ductile oceanic crust in the Ulleung Basin than under the Korean Peninsula. For the continental shelf and slope region between the Korean Peninsula and the Ulleung Basin, we estimate that V_s representing the Moho depth decreases from 4.0 to 3.75 km/s toward the Ulleung Basin.

At passive margins with voluminous igneous activity, the continent–ocean transition (COT) lies under the continental slope, where rapid crustal thinning occurs (Blaich et al., 2011 and references therein). Although the accurate crustal structure is difficult to image from surface waves, it is apparent that crustal thickness decreases rapidly under the epicentral area, marking the rifted (i.e., faulted) COT zone from the continental crust of the Korean Peninsula to the back-arc oceanic crust in the Ulleung Basin. It is well known that stress tends to increase at geometric discontinuities in stressed material (e.g., Durelli et al., 1978). In this regard, the epicentral area is susceptible to stress concentration that can induce frequent seismicity.

6. Identification of Faults and Folds in the Epicentral Area

6.1. Stratigraphy

The SE continental shelf of the Korean Peninsula has remained a major sediment source since the onset of back-arc rifting in the Late Oligocene, being underlain by a sedimentary succession up to over 11 km thick. Lee et al. (2011) identified a total of 12 sequence boundaries by correlating seismic sequences with biostratigraphic data from deep wells located on the shelf. In this study, we correlate seismic profiles with those in Lee et al. (2011) (Figs. 5, 6, 7, 8). Of the boundaries, UNC-01 and UNC-02 that are considered to be Pliocene are not constrained, due to the absence of biostratigraphic data.

Ingle (1992) and Lee and Kim (2002) derived the subsidence pattern of the continental shelf based on the analysis of subsidence and uplift at deep well sites on the SE coast of the Korean Peninsula and the continental shelf. The pattern indicates three
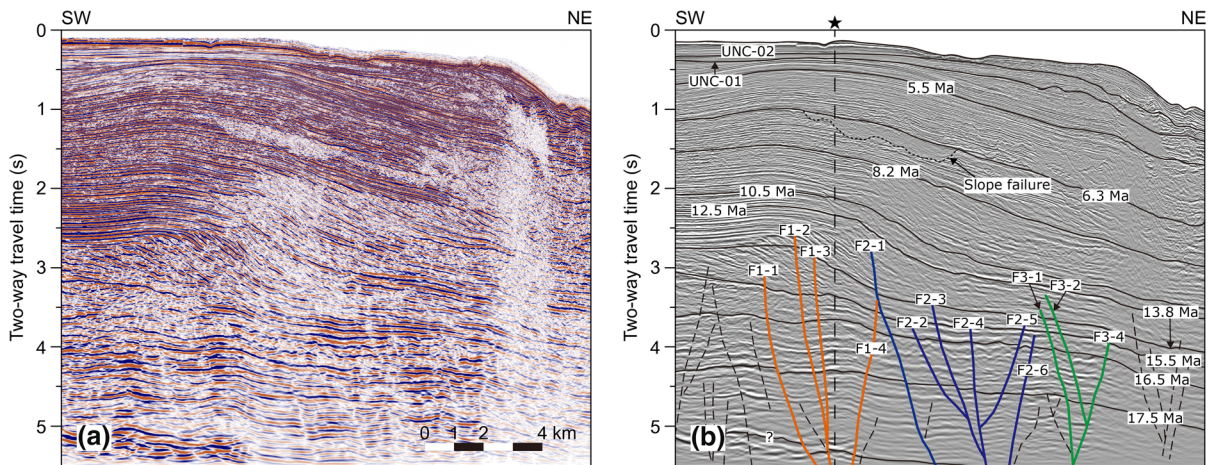
Figure 5
a Seismic profile crossing the epicentral area in a NE–SW direction and **b** its interpretation showing faults making up flower structures. UNC-01 and UNC-02 are unconformities possibly in the Pliocene sequences
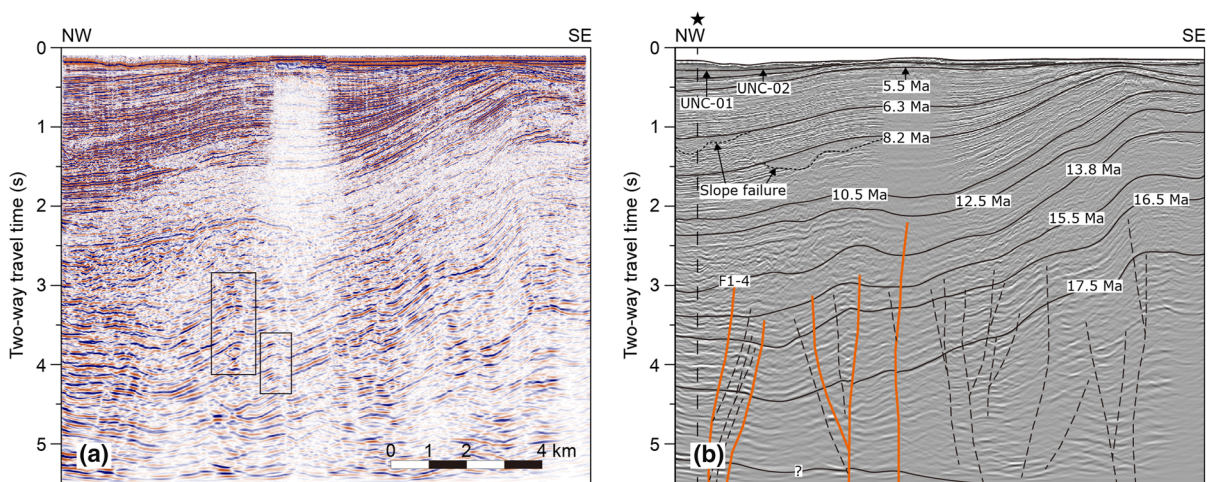

Figure 6
a Seismic profile crossing the epicentral area in a NW–SE direction and **b** its interpretation showing pop-up structures (in rectangles)

distinguished stages: (1) main tectonic subsidence from ~ 25 to ~ 12 Ma, (2) uplift from ~ 12 to ~ 10 Ma, and (3) relatively slow subsidence from ~ 10 Ma to the present. Back-arc rifting to spreading from the Late Oligocene to the Middle Miocene at the Korean margin pertains to the first stage of main tectonic subsidence.

The seismic sequences below the 16.5 Ma boundary consist of parallel-to-subparallel, high-amplitude reflectors that are likely to reflect uniform deposition in shallow-marine environments expected in the early

stage of subsidence (Figs. 5, 6, 7, 8). The overlying sequences between the 16.5 and 12.5 Ma boundaries were deposited in an overall sigmoidal shape, representing a shift to shelf margin deposition. The lower part of the sigmoid (from ~ 16.5 to 13.8 Ma) consists of oblique (or tangential) slope clinoforms that may occur in association with the shelf-margin deltas/shoreface deposits. The overlying sequences (from 13.8 to 12.5 Ma) are interpreted as slope clinoforms and turbidites. A submarine landslide recognized in Miocene sequences suggests that those
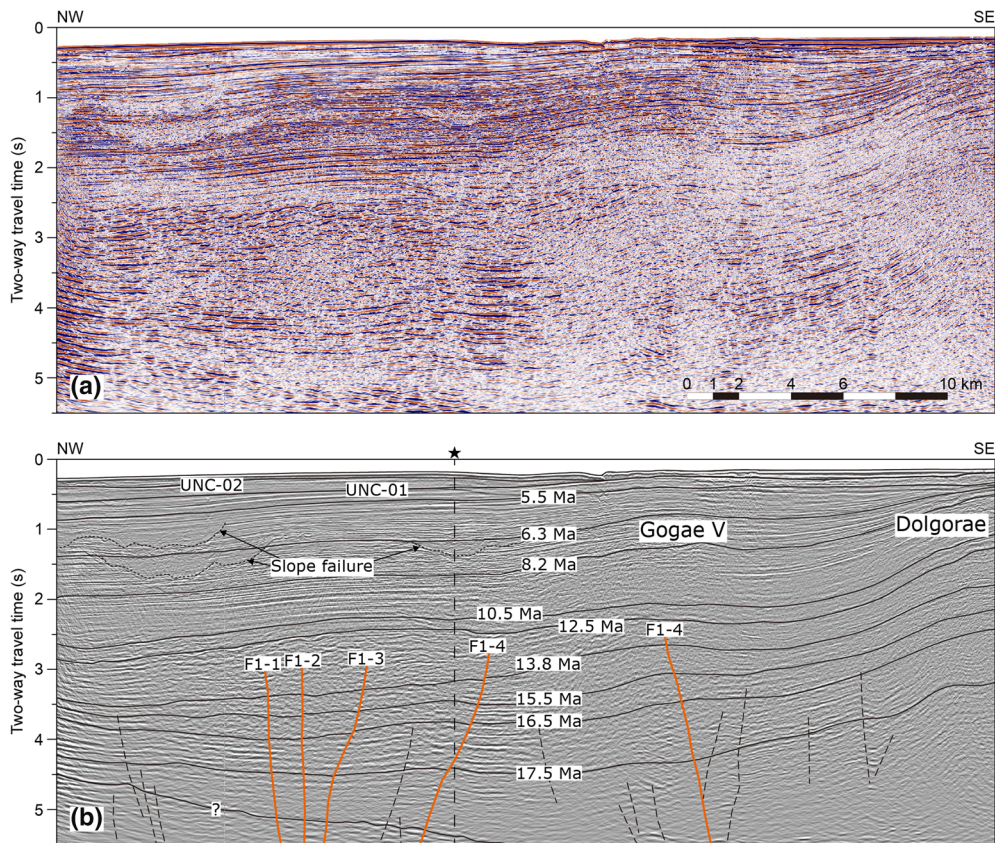
Figure 7

a Seismic profile V-1 showing anticlinal structures Gorae V and Dolgorae in a NW–SE direction and **b** its interpretive line drawings. The epicenter of the 2016 M_w 5.0 earthquake is above the Gorae V structure. See Fig. 3 for location

sequences experienced subsidence to the continental slope depth, and slope failures were possibly caused by the turbidite flow downslope. The sequences of the Middle Miocene to the present younger than 12.5 Ma largely show well-stratified and parallel layered reflectors, which are representative of marine sedimentation after back-arc spreading. Therefore, the external geometry and internal architecture of sedimentary sequences show correlation with the progressive (or temporal) subsidence associated with the separation of the SW Japan Arc.

6.2. Faulting in Sediments Deposited Since the Early Miocene

MCS profiles in this study, less than 5.5 s long in two-way travel time, do not include the basement rocks underlying sedimentary sequences; as a main reason, the overlying sediment cover at the continental shelf is too thick, thicker than 11 km in the depocenter, for the seismic pulses to penetrate into the underlying basement rocks. Therefore, the deformation of the basement rocks associated with back-arc rifting is not identified. However, the sedimentary sequences ranging from older than 17.5 Ma to the present enable us to identify faults and interpret their activity in the epicentral area.

Numerous faults are recognized on seismic profiles that displace stratigraphic sequences (Figs. 5, 6, 7, 8). Within the limit of resolution of seismic profiles, most of the faults do not clearly extend to shallow levels above the 12.5 Ma horizon. Because vertical displacement caused by the faults is not large, it is difficult to trace faults accurately. Nevertheless, the pre-15.5 Ma units show recognizable deformation caused by faulting. Overall, the faults are grouped
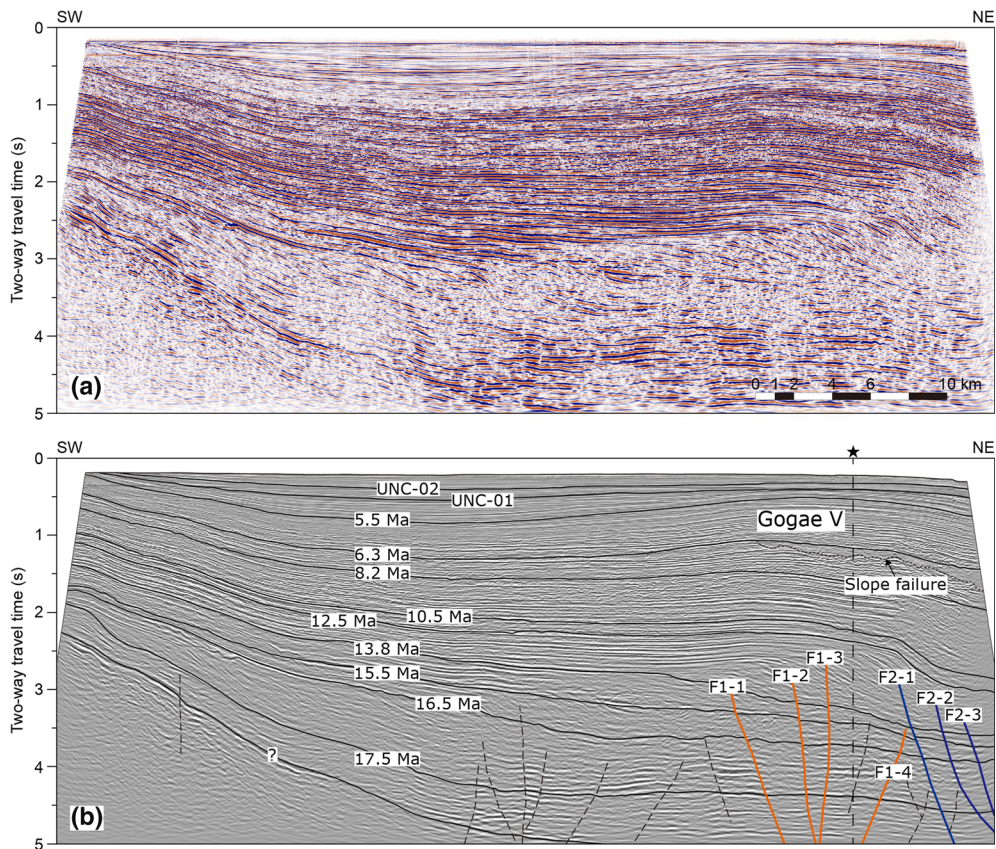
Figure 8
a Seismic profile V-2 showing anticlinal structure Gorae V in a NE–SW direction and **b** its interpretive line drawings. See Fig. 3 for location

into three structures with splays that diverge upwards, suggesting the characteristics of a flower structure (Fig. 5). Local pop-up structures created by compression are well recognized on the fault planes (Fig. 6). These features are representative of strike-slip faults. Other evidence for strike-slip faults described in Barnes and Audru (1999) includes (1) simultaneous development of normal and reverse offsets and (2) changes in the dip direction along the strike of individual fault splays. However, small vertical separation of stratigraphic reflectors by faults on seismic profiles in our study makes it difficult to clearly identify these features. We grouped faults into three flower structures of F1, F2, and F3. Individual faults are numbered so as to represent the flower structure that they belong to. For example, faults F1-1 to F1-4 belong to flower structure F1. The numbered faults are traced consistently on consecutive profiles.

Other disruptions suggestive of faulting but not traced on consecutive profiles are denoted by dashed lines on the profiles and are not named.

The F1 structure appears as a combination of a more evident positive flower structure between faults F1-3 and F1-4 and less evident negative structure between faults F1-2 and F1-3, implying the dominance of compressional stress. We infer that faults F1-3, F2-1 (and possibly F2-4), and F3-1 are main (or stem) faults of flower structures F1, F2, and F3, respectively, because they appear more vertical than other faults in respective structures and/or other faults appear to diverge away from them.

The eastern Korean continental margin north of the SE continental shelf consists of distinctive structural elements typical of a passive continental margin formed by continental rifting to spreading, although it is in the back-arc region (Kim et al.,

2015). In other words, the margin consists of a seaward succession of rifts, uplifted flanks, and a slope descending to the floor of the Ulleung Basin underlain by back-arc oceanic crust. The Hupo Fault is a major fault at the eastern Korean margin that controlled back-arc rifting (Fig. 1b) (Kim et al., 2007). The Hupo Fault, on the whole, is oriented N–S, with its southern portion striking NNE–SSW south of 36.5° N, implying that back-arc rifting controlled by the Hupo Fault commenced under E–W extension (Fig. 2a and b); later, back-arc spreading progressed with the separation of the SW Japan Arc principally to the southeast (Fig. 2c) (Kim et al., 2015 and references therein).

Figure 9 shows the traces of faults on the 16.5 Ma stratigraphic boundary in the epicentral area of the 2016 M_w 5.0 earthquake. The faults in the F1 group and fault F2-1 typically consist of linear northern and southern portions trending NNE–SSW and NW–SE, respectively. The NNE–SSW strike of the northern portion is identical to that of the southern part of the Hupo Fault and the inferred locus of breakup along the slope base (Kim et al., 2015) (Fig. 1b). As described previously, the SE continental shelf and slope region is rifted continental crust. We thus interpret that the NNE–SSW-striking northern portion of the faults in the epicentral area was created by extension either by the same back-arc rifting process
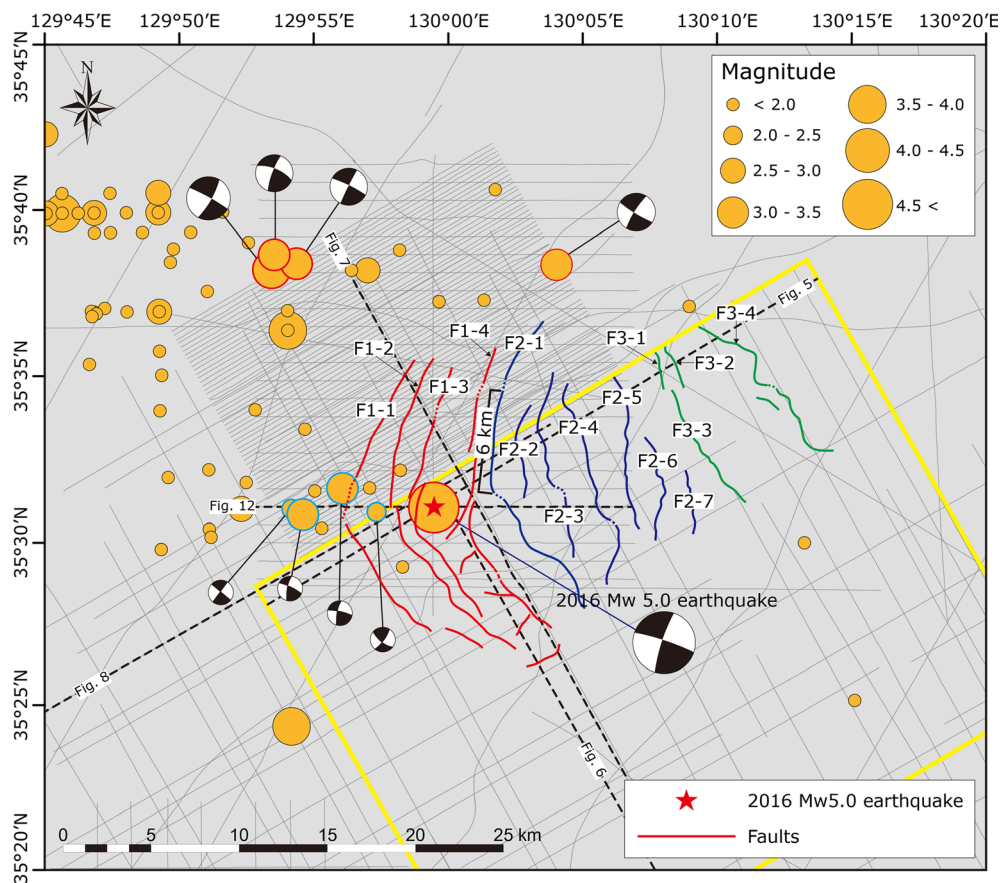

Figure 9
Fault traces on the 16.5 Ma boundary in the epicentral area of the 2016 M_w 5.0 earthquake. The focal mechanism solutions of the four events denoted by green circles in the epicentral area of the 2016 M_w 5.0 earthquake are from Hong et al. (2020). Note that the faults in the F1 group and F2-1 typically consist of northern and southern portions striking NNE–SSW and NW–SE, respectively. The dotted lines represent the locations of seismic profiles labeled with a figure number in the text. The yellow rectangle denotes the area of 3-D seismic data acquisition

as in the eastern margin of the Korean Peninsula or during ensuing back-arc spreading in the Ulleung Basin. Inferred stem faults such as F2-1 and F3-1 show normal slip, with a down-to-the NE sense of displacement (Fig. 5) below the 17.5 Ma horizon. Because seismic profiles do not show sequences much deeper than 17.5 Ma, the sense of slip in the Late Oligocene to earliest Miocene deposits is difficult to determine. However, the thickening of stratal units in the hanging wall blocks below the 17.5 Ma horizon (Fig. 5) indicates that these faults accommodated extensional deformation in the Early Miocene and possibly earlier, being consistent with the age of back-arc rifting to spreading.

6.3. Anticline Structures

There are two anticlinal structures in the epicentral area trending NE–SW and NNW–SSE, respectively (Figs. 1b, and 5, 6, 7, 8). The NE–SW-trending anticline structure, termed the Dolgorae structure, comprises a series of thrusts and anticlines (Lee et al., 2011). The Dolgorae structure is a NW reach of the San-in Fold Zone emplaced along the continental shelf of the SW Japan Arc. The Dolgorae structure resulted from back-arc closing under northward compression induced by the contact of the Philippine Sea Plate with the SW Japan Arc (Fig. 2d) (Lee et al., 2011). The much shorter and narrower NNW–SSE-trending anticline indicative of ENE–WSW compression, termed the Gorae V structure, is orthogonal to the Dolgorae structure. Lee et al. (2011), based on structural mapping and cross-section restoration of seismic profiles, suggested that crustal shortening to create the Dolgorae structure began sometime between the latest Early (16.5 Ma) and the earliest Middle Miocene (15.5 Ma) and ceased later than 6.3 Ma, whereas the central part of the Gorae V anticline has grown relatively rapidly until very recently since the early Late Miocene (10.5–8.2 Ma). They further suggested that the stress regime in the back-arc changed rapidly from NNW–SSE compression to ENE–WSW (or E–W) compression after 5.5 Ma, resulting in the NNW–SSE-trending, additional growth of the Gorae V structure.

The epicenter of the 2016 M_w 5.0 earthquake is in the northern distal end of the Gorae V structure. We conducted balanced cross-section restoration of two mutually perpendicular seismic profiles V-1 (Fig. 7) and V-2 (Fig. 8) that pass close to the epicenter in the NNW–SSE and ENE–WSW directions (Fig. 3), respectively, with the objectives (1) to construct a model for the geological evolution of the epicentral area and (2) to see whether the epicentral area evolved under the present ENE–SWS compression. A total of 12 sequence boundaries identified on seismic profiles were reconstructed, including the seafloor as the top boundary and the pre-17.7 Ma sequence as the lowermost sequence. We followed the restoration procedure in Lee et al. (2011) using the same parameters therein. In the restoration, faults were not considered because (1) the restoration method is a 2-D scheme and (2) vertical displacement by faulting is small and not clearly recognized above the 12.5 Ma horizon, and (3) faulting had little effect on the growth of the Gorae anticline.

Profile V-1 is 36 km long, extending along the axial trace of the Gorae V structure lengthwise in the SSE direction and further into the northern part of the Dolgorae structure (Fig. 7). Restoration of profile V-1 demonstrates rapid subsidence and thick accumulation of sediments earlier than 16.5 Ma (Fig. 10) that signify extension associated with a significant component of normal faulting while back-arc spreading took place in the main part of the Ulleung Basin to the north. The anticlinal growth of the Dolgorae structure began earlier than 12.5 Ma and persisted to later than 8.2 Ma. The Gorae V structure emerged coevally with the Dolgorae structure with much smaller amplitude, but did not gain additional growth after 8.2 Ma recognizably.

Profile V-2, 49 km long, shows the structure of the northern tip of the Gorae V anticline that includes the epicentral area of the 2016 M_w 5.0 earthquake (Fig. 8). The Gorae V anticlinal structure on profile V-2, unlike the central part of the Gorae V structure on profile V-1, did not grow before 8.2 Ma but commenced after 5.5 Ma (Fig. 11) with the axial trace trending NNW–SSE, implying additional growth under ENE–WSW compression. The additional growth of the Gorae V anticline in the epicentral area after 5.5 Ma is recognized not on profile V-1 in the NNW–SSE direction but on profile V-2 in the ENE–WSW, which corroborates
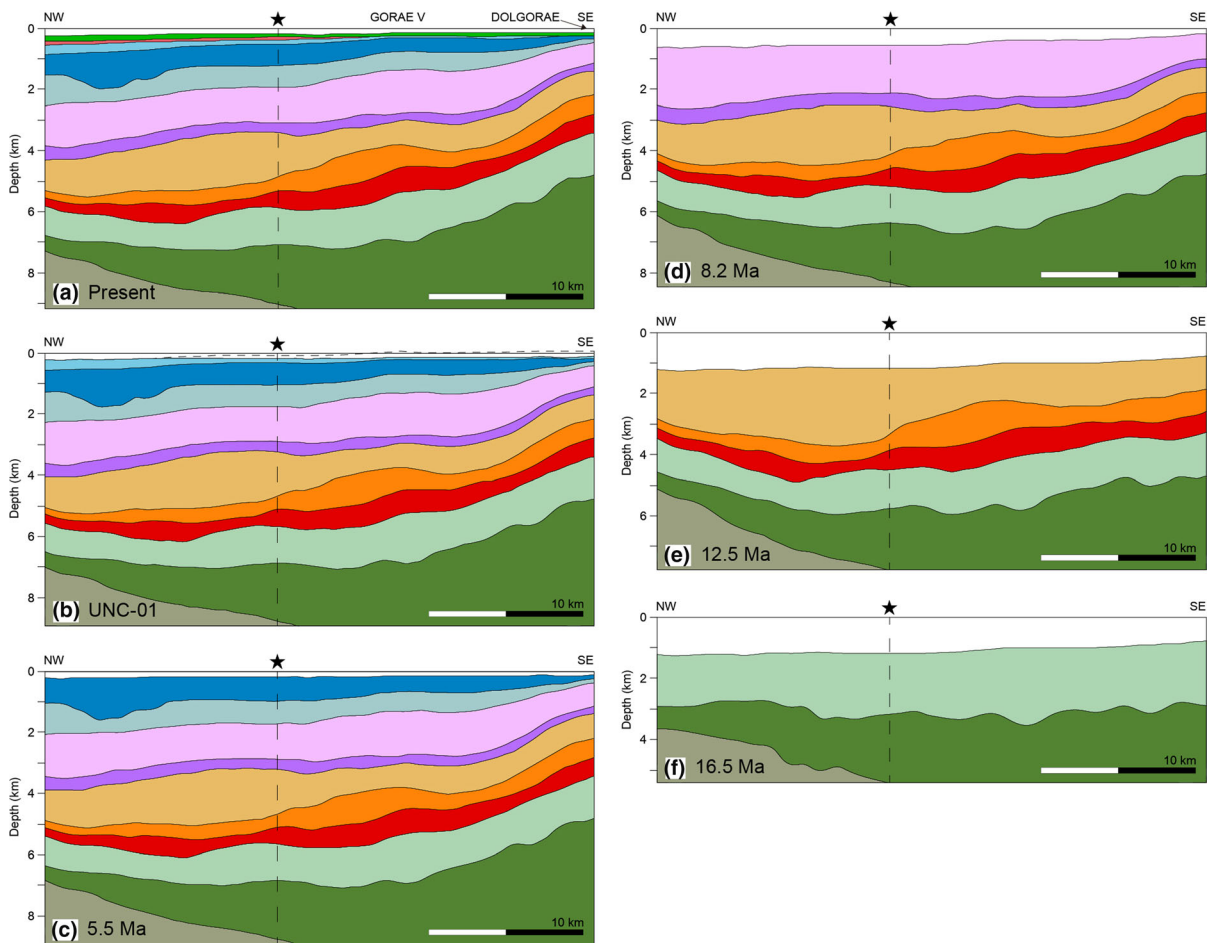
Figure 10
Sequential restoration of depth model of profile V-1. The star denotes the epicenter of the 2016 M_w 5.0 earthquake

compression in the ENE–WSW direction. It thus appears that the ongoing geological deformation of the epicentral area is not directly tied to compression from the collision of the Philippine Sea Plate with the SW Japan Arc, although the collision induced NNW–SSE (or N–S) compression on the back-arc continental shelf between the Korean Peninsula and the SW Japan Arc.

Sparker profiles show the structure of the upper part of the Gorae V anticline and overlying sediments with much higher resolution than air gun profiles (Fig. 12). Notably, the UNC-01 horizon within the Gorae V anticline was eroded in the hinge zone, which suggests that the growth of the Gorae V structure persisted until recently in the epicentral area

of the 2016 M_w 5.0 earthquake and resulted in erosion on the seafloor possibly combined with sea level fall. The internal stratal units below the UNC-01 horizon maintain their thickness individually whether they are in the hinge zone or in the limb. In contrast, the layers above the UNC-01 horizon are characterized by a thinning upward pattern, particularly noticeable between the UNC-01 and the UNC-02, being characteristic of growth strata. Consequently, we think that the additional growth of the Gorae V structure in the epicentral area commenced later than 5.5 Ma in the Pliocene. The large erosional hollow on the seafloor in the crestal area of the fold was formed by enhanced currents that flowed along the seafloor during the Last Glacier Maximum (LGM) (Cukur
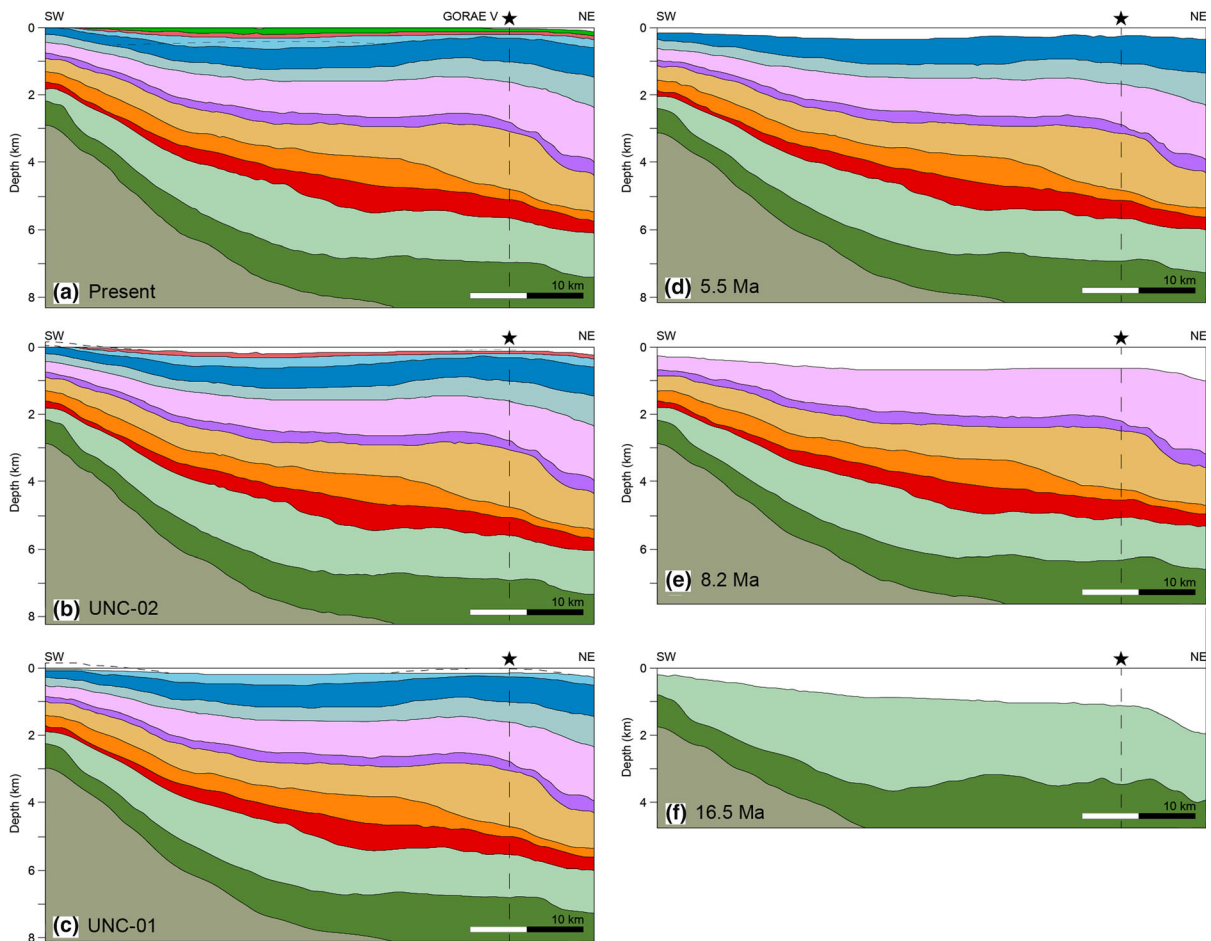
Figure 11
Sequential restoration of depth model of profile V-2. The star denotes the epicenter of the 2016 M_w 5.0 earthquake

et al., 2019) when the sea level was lower by $\sim$ 130 m from the present level (Fig. 12).

7. Discussion on Neotectonics

7.1. Fault Structures Correlated with Seismicity

The northern part of fault groups F1 and F2 striking NNE–SSW (Fig. 9) will have right-lateral displacement under the present ENE–WSW-oriented compressive stress field, which is consistent with the fault plane solution of the 2016 M_w 5.0 earthquake demonstrating NNE–SSW strike-slip with a rake angle of 174°. Considering the focal mechanism

solution consistent with the fault geometry in the epicentral area, we think that the fault in the basement that generated the 2016 M_w 5.0 earthquake has similar geometry. The rake angle of 174° implies nearly pure strike-slip on the causative fault. We, therefore, propose that the 2016 M_w 5.0 earthquake occurred due to compressional reactivation of a fault underlying the F1 fault group that encompasses the epicenter (Fig. 9). Microseismicity in the epicentral area of the 2016 M_w 5.0 earthquake also has focal mechanism solutions indicating NNE–SSW strike-slip (Fig. 9) (Hong et al., 2020) which are in good agreement with the geometry of the F1 fault structure. Taken together, this suggests to us a primary
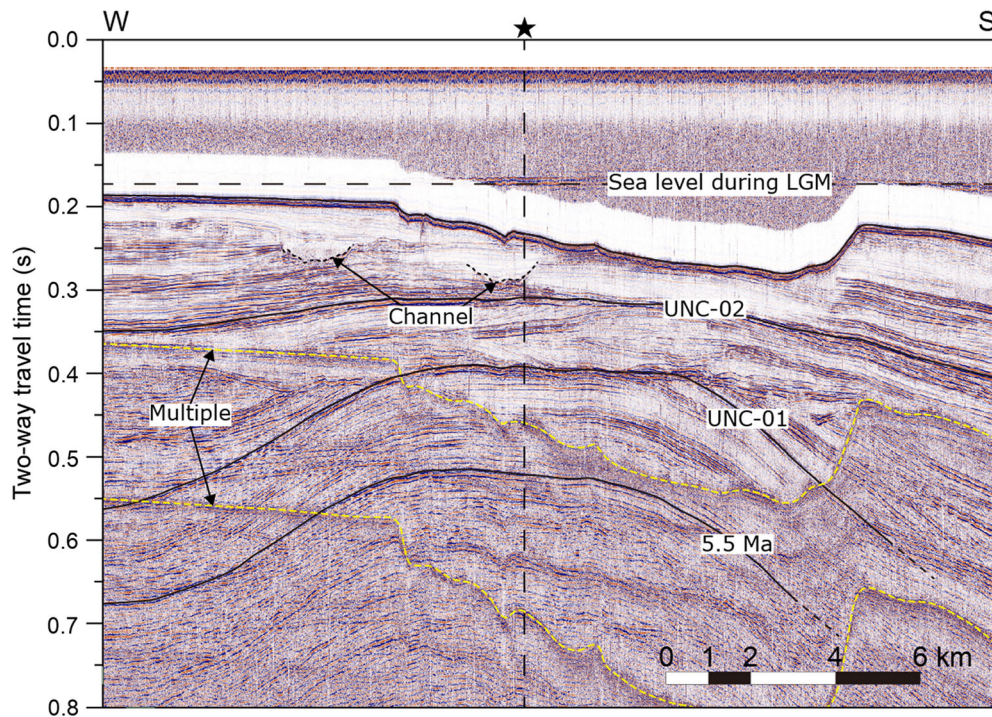
Figure 12
Sparker profile showing the sedimentary structure of the Gorae V anticline. The star denotes the epicenter of the 2016 M_w 5.0 earthquake. See Fig. 3 for location

relationship between the current seismicity and the faults in the epicentral area of the 2016 M_w 5.0 earthquake. More specifically, we interpret the F1 fault system encompassing the epicentral area as the source structure of the earthquake.

Faults, however, are not recognized in sedimentary sequences overlying the 12.5 Ma horizon on MCS and sparker profiles. We think of several possibilities: (1) it may be difficult for strike-slip to generate a recognizable vertical displacement in horizontally layered sequences within the resolution of seismic profiles; (2) the magnitude of earthquakes mostly less than M_w 5.0 is not large enough to displace water-saturated sediments that tend to behave plastically; and (3) the faulted sedimentary structure was not preserved due to repeated slope failures when the seafloor subsided to the level of the continental slope.

We mentioned previously that the SW Japan Arc was pushed northward during back-arc closing after ~ 15 Ma by the northward-advancing

Philippine Sea Plate (Fig. 2d). Kim et al. (2008), based on the analysis of paleo-stress in Oligocene to Miocene times in Tsushima Island located on the continental shelf between the Korean Peninsula and the SW Japan Arc (Fig. 1b), suggested that the SW Japan Arc rotated rapidly clockwise while it was pushed northward (Fig. 2d). We do not know whether the NW–SE strike of the southern portions of fault groups F1 and F2 resulted from this process. If so, the southern portions may mark the northward reach of deformation by back-arc closing under NNW–SSE (or N–S) compression behind the SW Japan Arc.

We statistically estimate M_{max} at the continental margin between the Korean Peninsula and the SW Japan Arc using the recorded earthquakes (Fig. 1). For estimation, HA3 software (Kijko et al., 2016) is used, which is useful for an incomplete seismic catalog for a specified region. HA3 software computes M_{max} values by eight procedures depending on the statistical distribution of earthquake magnitudes. The earthquakes have been instrumentally recorded

with their magnitude on the local scale (M_L) by the KMA since 1981. Most of the recorded earthquakes are less than M_L 4.0.

Sheen et al. (2018) showed that the ratio of the M_w/M_L averages to 1.0 in and around the Korean Peninsula. Therefore, we assume that M_L can be used as M_w without converting the magnitude values (Figs. 1 and 9). The M_{max} ranges from M_w 5.15 ± 0.16 to 5.72 ± 0.72, averaging 5.44 ± 0.45 (Table 1), with lower and upper limits of 4.99 and 5.99, respectively. We note that the Tate-Pisarenko procedure failed to compute M_{max}, which may be due to the limited number of relatively large-magnitude earthquakes recorded in a short time span, leading to the inability to compute an estimator for the procedure.

Anderson et al. (1996) derived an empirical relationship between the potential magnitude of earthquakes and the fault length. Strike-slip faults are normally divided into segments bounded by fault bends and step-overs. However, it is difficult to define individual segments of the faults in fault groups F1, F2, and F3 because these faults are characterized by abundant bending (Fig. 9); in addition, large earthquakes with aftershocks have not occurred for us to trace the length of a source fault in the study area. The fault length capable of generating a M_w 5.99 earthquake is calculated as 5.6 km using the relationship in Anderson et al. (1996, Eq. 3). If a straight portion of a fault bounded by recognizable bends is regarded as a fault segment in the study area, the fault

segments in the F1 and F2 fault groups appear to be less than 6 km in length, which is roughly compatible with the fault length calculated from M_{max}. It is thus likely that M_{max} in the epicentral area and possibly at the SE continental margin of the Korean Peninsula is not higher than M_w 6.0.

7.2. Origin of the Stress Field in and Around the Korean Peninsula

The focal mechanism solutions of the earthquakes in and around the southern Korean Peninsula indicate the maximum compressive stress in the ENE–WSW direction (e.g., Rhie & Kim, 2010). The subduction of the Pacific and Philippine Sea Plates under the Japan Arc does not appear to contribute directly to this ENE–WSW compressive stress, because they are subducting in the NW direction (e.g., Holt et al., 2018).

Xu et al. (1992) analyzed earthquake data in China and suggested that the maximum principal compressive stress axis is approximated by the mean P-axis that follows a radial pattern induced by the continental collision between the Indian and Eurasian Plates (Fig. 13). Park et al. (2006) noted that the directions of maximum horizontal stress in the southern Korean Peninsula inferred from the analysis of Quaternary faults follow approximately the projection of the mean P-axis from China (Fig. 13). Consequently, the authors suggested that the India–Asia continental collision is the main source of the stress field in the SE Korean Peninsula.

Choi et al. (2012) computed the P-axis direction in and around the Korean Peninsula from earthquake data. The P-axis is oriented E–W or ENE–WSW at the eastern and SE continental margin of the Korean Peninsula, whereas the P-axis is oriented more or less WNW–ESE at the northern margin, which is difficult to explain by the projection of the mean P-axis from China (Fig. 13). Furthermore, observation and modeling of the deformation of Asia suggested that the zone of deformation directly related to the India–Eurasia collision is much smaller than originally predicted (e.g., Keary et al., 2009), implying that the stress field in and around the Korean Peninsula may not result entirely from the collision.

Table 1

The maximum magnitude of earthquakes (M_{max}) expected at the SE continental margin of the Korean Peninsula computed by HA3 software (Kijko et al., 2016)

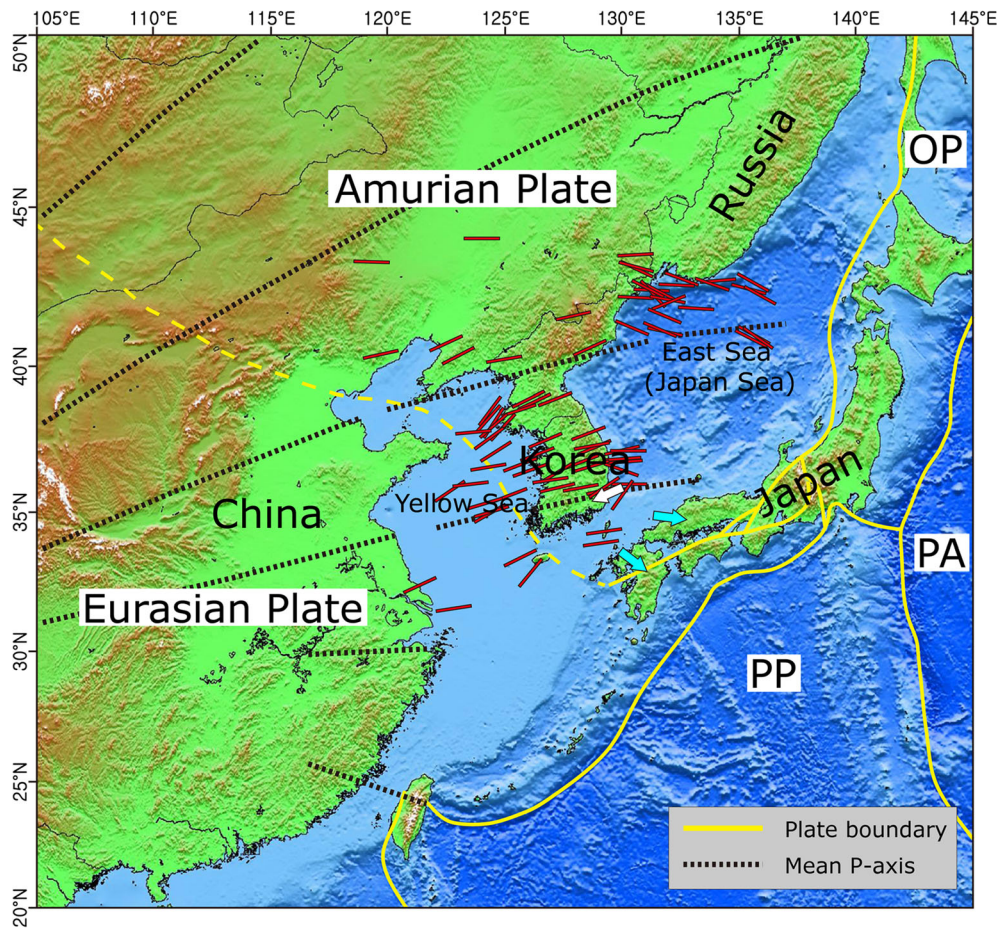| Procedures	M_{max} (M_w)
Maximum likelihood	5.15 ± 0.16
Gibowicz-Kijko	5.72 ± 0.72
Gibowicz-Kijko-Bayes	5.44 ± 0.44
Kijko-Sellevoll	5.50 ± 0.50
Kijko-Sellevoll-Bayes	5.37 ± 0.38
Tate-Pisarenko	Failed
Tate-Pisarenko-Bayes	5.62 ± 0.62
Non-parametric (Gaussian)	5.31 ± 0.32
Average	5.44 ± 0.45

Figure 13

The mean P-axis trajectories in east Asia created by India–Asia collision compiled from Xu et al. (1992) and Park et al. (2006). The P-axis orientations (red bars) in and around the Korean Peninsula are from Choi et al. (2012). The white and cyan arrows represent the present direction of compression at the Korean margin (Kim et al., 2016) and the deformation on the back-arc side of the SW Japan Arc (Nishimura & Takada, 2017), respectively

Lee et al. (2011) suggested that the eastward movement of the Amurian Plate induces the ENE–WSW compression at the continental margin of the Korean Peninsula. This suggestion poses a problem because the growth of the Gorae V structure is too local to be explained by plate motion. In addition, an appropriate explanation is not given for the occurrence of the Gorae V anticline in the interior of the Amurian Plate and not on its boundary.

In the SE Korean Peninsula, the NNE-trending Yangsan Fault is the most prominently defined structure (Fig. 1b), with essentially dextral activity from the Eocene to the Quaternary (Kim et al., 2016). A recent study on structural geology and age reported

that dextral slip on the Yangsan Fault ceased at 25 Ma (or 23 Ma), then resumed under the present ENE–WSW compressional stress (Cheon et al., 2017). This indicates that (1) the Yangsan Fault was not activated dextrally during the main phase of back-arc rifting and spreading from the Late Oligocene to the Middle Miocene and subsequent back-arc closing induced by northward compression from the Middle Miocene, and (2) the resumption of dextral slip on the Yangsan Fault began later than 5.5 Ma under ENE–WSW compression (more specifically compression toward the WSW), as deduced from the restoration of the epicentral area. Consequently, we think that the generation of the stress
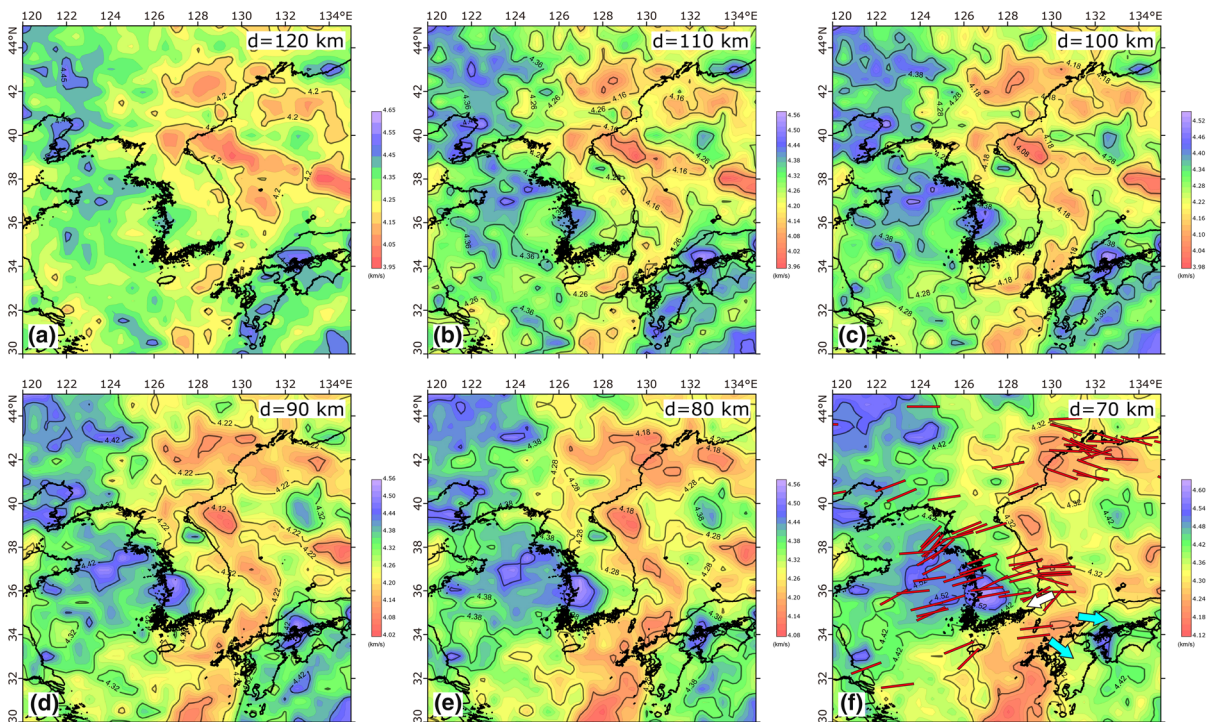
Figure 14
Horizontal slices of V_s (km/s) at depths of **a** 120, **b** 110, **c** 100, **d** 90, **e** 80, **f** 70 km. The P-axis orientations (red bars) in and around the Korean Peninsula are from Choi et al. (2012). The white and cyan arrows represent the present direction of compression at the Korean margin (Kim et al., 2016) and the deformation on the back-arc side of the SW Japan Arc (Nishimura & Takada, 2017), respectively

field in the SE Korean Peninsula is tied to the tectonic activity at the continental margin of the Korean Peninsula.

A dense grid of GNSS (Global Navigation Satellite System) data indicates that the dominant compressional deformation on the back-arc side of the SW Japan Arc is oriented SSE (or SE) (Nishimura & Takada, 2017) (Fig. 13). Considering the compression at the continental margin of the Korean Peninsula toward WSW, it appears that the compressional stress at the continental margin of the Korean Peninsula and its conjugate margin of the SW Japan Arc originates from the back-arc region between the two margins, not from the far-field stress generated at plate boundaries. The maximum horizontal stress in the Korean Peninsula decreases rapidly from the east coast toward the western part of the peninsula (Soh et al., 2018). This decrease is not explained by far-field stress, either; rather, it may result from a near-field stress origin, being consistent with the stress

from the back-arc region. The subducting Pacific Plate is dipping under the bac-arc side of the SW Japan Arc and becomes flat before reaching the Korean Peninsula toward mainland Asia (e.g., Kim et al., 2016). The Philippine Sea Plate is also subducting under the SW Japan Arc and extends to the back-arc side of the SW Japan Arc (e.g., Zhao et al., 2021). Asthenospheric upwelling is easily induced above the dipping subducting plate (Conder et al., 2002) which can also be a source of the low velocities at the SW Japan margin.

The V_s structure from ambient noise tomography shows low-velocity anomalies in the shallow mantle at the continental margins of the Korean Peninsula and the SW Japan Arc (Fig. 14). The anomalies at the continental margin of the Korean Peninsula were interpreted as waning mantle upwelling induced in the mantle wedge above the subducted oceanic lithosphere during back-arc rifting and spreading in a region of hotter than normal mantle temperature

(Kim et al., 2015) or a small-scale mantle convection unrelated to subduction (Lü, 2019). Asthenospheric upwelling after the cessation of back-arc spreading in the back-arc region is supported by the age and geochemistry of basalt sampled from the Seifu Seamount in the NE part of the Ulleung Basin (Morishita et al., 2020). The low-velocity anomalies, representing convection in the uppermost mantle, advance laterally toward the basal lithosphere of the peninsula as they rise upward. These low-velocity anomalies at 70–80 km depth, in particular, appear as a unit elongated along the continental margin of the Korean Peninsula; the P-axis direction at the margin agrees fairly well with the inferred advancing direction of these anomalies. We estimate that the convection in the uppermost mantle can exert compressive stress on the thick continental lithosphere of the Korean Peninsula by directing the convective flow toward the peninsula. Small-scale, edge-driven convection that develops in the upper mantle beneath the transition of thick cratonic lithosphere and thin oceanic lithosphere (King & Ritsema, 2000) is a model to drive mantle convection toward the thick lithosphere at the upper boundary of a convection cell. The thick and cold continental lithosphere and the thin and hot oceanic lithosphere at the continental margin of the Korean Peninsula may offer conditions favorable for shallow mantle convection.

We, therefore, interpret that the uppermost mantle convection plays an important role in generating the present stress field at the continental margin of the Korean Peninsula, although there may be other background contributions such as far-field stress from plate boundaries. Because intraplate stress sources can control the plate-scale stress field caused by plate boundary forces (Heidbach et al., 2007), further studies are needed to understand the stress field at the back-arc continental margins of the Korean Peninsula and the Japan Arc, where the interplay of various stress sources is suggested (Lallemand et al., 2005).

8. Conclusions

The SE continental margin of the Korean Peninsula evolved with crustal extension and shortening during back-arc rifting and closing, respectively, commencing in the Late Oligocene. Based on the analysis of seismic reflection profiles combined with inferred crustal structure, we correlated the occurrence of the 2016 M_w 5.0 earthquake at the margin with geological structure. The conclusions of our study are as follows:

1. The margin includes a transition zone from rifted continental crust of the Korean Peninsula to back-arc oceanic crust underlying the Ulleung Basin, characterized by a rapid decrease in crustal thickness.
2. The epicentral area of the 2016 M_w 5.0 earthquake is in the northern tip of an anticline created by ENE–WSW compression that commenced later than 5.5 Ma.
3. Abundant faults striking NNE–SSW were identified on seismic reflection profiles in the epicentral area that make up strike-slip fault systems. We suggest that extensional faults inherited from back-arc rifting are reactivated as strike-slip fault systems with dextral slip under the present ENE–WSW-oriented compressional stress at the margin.
4. Asthenospheric upwelling recognized in the uppermost mantle and elongated along the continental margin is inferred to induce a significant portion of the present ENE–WSW compressional stress.
5. The maximum magnitude of earthquakes expected in the epicentral area of the 2016 M_w 5.0 earthquake is estimated as no higher than M_w (or M_L) 6.0.

Funding

Availability of data

MCS profiles from KIOST are available upon request.

Declarations

REFERENCES

Anderson, J. G., Wesnousky, S. G., & Stirling, M. W. (1996). Earthquake size as a function of fault slip rate. *Bulletin of the Seismological Society of America, 86*, 638–690.

Barnes, P. M., & Audru, J.-C. (1999). Recognition of active strike-slip faulting from high-resolution marine seismic reflection profiles, Eastern Marlborough fault system, New Zealand. *Bulletin of the Seismological Society of America, 111*, 538–559.

Blaich, O. A., Faleide, J. I., & Tsikalas, F. (2011). Crustal breakup and continent-ocean transition at South Atlantic margins. *Journal of Geophysical Research, 116*, B01401. https://doi.org/10.1029/2010JB007686

Carcione, J., & Poletto, F. (2013). Seismic rheological model and reflection coefficients of the brittle–ductile transition. *Pure and Applied Geophysics, 170*, 2021–2035.

Cheon, Y., Ha, S., Lee, S., Cho, H., & Son, M. (2017). Deformation features and history of the Yangsan Fault Zone in the Eonyang-Gyeongju area, SE Korea. *Journal of the Geological Society Korea, 53*, 95–114.

Cho, H. M., Baag, C. E., Lee, J. M., Moon, W., Jung, H., Kim, K. Y., & Asudeh, I. (2006). Crustal velocity structure across the southern Korean Peninsula from seismic refraction survey. *Geophysical Research Letters, 33*, L06307. https://doi.org/10.1029/2005GL025145

Choi, H., Hong, T. K., He, X., & Baag, C. E. (2012). Seismic evidence for reverse activation of a paleo-rifting system in the East Sea (Sea of Japan). *Tectonophysics, 572–573*, 123–133.

Conder, J. A., Wiens, D. A., & Morris, J. (2002). On the decompression melting structure at volcanic arcs and back-arc spreading centers. *Geophysical Research Letters, 29*, GL015390.

Cukur, D., Kong, G. S., Chun, J. H., Kang, M. H., Um, I. K., Kwon, T. K., Johnson, S. Y., & Kim, K. O. (2019). Morphology and genesis of giant seafloor depressions on the southeastern continental shelf of the Korean Peninsula. *Marine Geology, 415*, 105966. https://doi.org/10.1016/j.margeo.2019.105966

Durelli, A. J., Brown, K., & Yee, P. (1978). Optimization of geometric discontinuities in stress fields. *Experimental Mechanics, 18*, 303–308.

Hall, R., Ali, J., Anderson, C. D., & Baker, S. (1995). Origin and motion history of the Philippine Sea Plate. *Tectonophysics, 251*, 229–250.

Hardebeck, J., & Shearer, P. M. (2003). Using S/P amplitude ratios to constrain the focal mechanisms of small earthquakes. *Bulletin of the Seismological Society of America, 93*, 2434–2444. https://doi.org/10.1785/0120020236

Heidbach, O., Reinecker, J., Tingay, M., Muller, B., Sperner, B., Fuchs, K., & Wenzel, F. (2007). Plate boundary forces are not enough: Second- and third-order stress patterns highlighted in the World Stress Map database. *Tectonics, 26*, TC6014. https://doi.org/10.1029/2007TC002133

Hisada, K.-I., Takashima, S., Arai, S., & Lee, Y. I. (2008). Early Cretaceous paleogeography of Korea and Southwest Japan inferred from occurrence of detrital chromian spinels. *Island Arc, 17*, 471–484.

Holt, A. F., Royden, L. H., Becker, T. W., & Faccenna, Cl. (2018). Slab interactions in 3-D subduction settings: The Philippine Sea Plate region. *Earth and Planetary Science Letters, 489*, 72–83. https://doi.org/10.1016/j.epsl.2018.02.024

Hong, T. K., Park, S., Lee, J., & Kim, W. (2020). Temporal seismicity evolution and seismic hazard potentials in the western East Sea (Sea of Japan). *Pure and Applied Geophysics*. https://doi.org/10.1007/s00024-020-02479-z

Horozal, S., Lee, G. H., Yi, B. Y., Yoo, D. G., Park, K. P., Lee, H. Y., Kim, W., Kim, H. J., & Lee, K. (2009). Seismic indicators of gas hydrate and associated gas in the Ulleung Basin, East Sea (Japan Sea) and implications of heat flows derived from depths of the bottom-simulating reflector. *Marine Geology, 258*, 126–138.

Hoshi, H. (2018). Miocene clockwise rotation of Southwest Japan. *Journal of the Geological Society of Japan, 124*, 675–691.

Ingle Jr., J.C. (1992). Subsidence pattern of the Japan Sea: stratigraphic evidence from ODP sites and onshore sections. In K. Tamaki, K. Suyehiro, J. Allan, & M. McWilliams (Eds.), *Proceedings of ODP Scientific Results* (Vol. 127/128, pp.1197–1218).

Jolivet, L., Shibuya, H., & Fournier, M. (1995). Paleomagnetic rotations and the Japan Sea opening. Active Margins and Marginal Basins of the Western Pacific. *Geophysical Monograph, 88*, 355–369.

Jolivet, L., Tamaki, K., & Fournier, M. (1994). Japan Sea, opening history and mechanism: A synthesis. *Journal of Geophysical Research, 99*, 22237–22259.

Jun, M. S. (1991). Body-wave analysis for shallow intraplate earthquakes in the Korean peninsula and Yellow Sea. *Tectonophysics, 192*, 345–357.

Keary, P., Klepeis, K. A., & Vine, F. J. (2009). *Global tectonics* (p. 482). Wiley-Blackwell.

Kijko, A., Smit, A., & Sellevoll, M. A. (2016). Estimation of hazard parameters from incomplete data files: Part III. Incorporation of uncertainty of earthquake-occurrence model. *Bulletin of the Seismological Society of America, 106*, 1210–1222. https://doi.org/10.1785/0120150252

Kilb, D., & Hardebeck, J. (2006). Fault parameter constraints using relocated earthquakes: A validation of first-motion focal-mechanism data. *Bulletin of the Seismological Society of America, 96*, 1140–1158. https://doi.org/10.1785/0120040239

Kim, G. B., Yoon, S. H., Kim, S. S., & So, B. D. (2018). Transition from buckling to subduction on strike-slip continental margins: Evidence from the East Sea (Japan Sea). *Geology, 46*, 603–606. https://doi.org/10.1130/G40305.1

Kim, H. J., Jou, H. T., Cho, H. M., Bijwaard, H., Sato, T., Hong, J. K., Yoo, H. S., & Baag, C. E. (2003). Crustal structure of the continental margin of Korea in the East Sea (Japan Sea) from deep seismic sounding data: Evidence for rifting affected by the hotter than normal mantle. *Tectonophysics, 364*, 25–42.

Kim, H. J., Jou, H. T., & Lee, G. H. (2018). Neotectonics of the eastern Korean margin inferred from back-arc rifting structure. *Ocean Science Journal, 53*, 601–609.

Kim, H. J., Lee, G. H., Choi, D. L., Jou, H. T., Li, Z., Zheng, Y., Kim, G. Y., Lee, S. H., & Kwon, Y. K. (2015). Back-arc rifting in the Korea Plateau in the East Sea (Japan Sea) and the separation of the SW Japan Arc from the Korean margin. *Tectonophysics, 638*, 147–157.

Kim, H. J., Lee, G. H., Jou, H. T., Cho, H. M., Yoo, H. S., Park, G. T., & Kim, J. S. (2007). Evolution of the eastern margin of Korea: Constraints on the opening of the East Sea (Japan Sea). *Tectonophysics, 436*, 37–55.

Kim, H. J., Moon, S., Jou, H. T., Lee, G. H., Yoo, D. G., Lee, S. H., & Kim, C. H. (2016). The offshore Yangsan Fault activity in the Quaternary: Analysis of high-resolution seismic profiles. *Tectonophysics, 693*, 85–95.

Kim, H. G., Song, C. W., Kim, J. S., Son, M., & Kim, I. S. (2008). Tertiary geological structure and deformation history of southern Tsushima Island. Japan. *Journal of the Geological Society of Korea, 44*, 175–198.

Kim, K. H., & Park, Y. (2010). The 20 January 2007 M_L 4.8 Odaesan Earthquake and its implications for regional tectonics in Korea. *Bulletin of the Seismological Society of America, 100*, 1395–1405. https://doi.org/10.1785/0120090234

Kimura, J.-I., Stern, R. J., & Yoshida, T. (2005). Reinitiation of subduction and magmatic responses in SW Japan Arc during Neogene time. *Geological Society of America Bulletin, 117*, 969–986. https://doi.org/10.1130/B25565

King, S., & Ritsema, J. (2000). African hot spot volcanism: Small-scale convection in the upper mantle beneath cratons. *Science, 290*, 1137–1140. https://doi.org/10.1126/science.290.5494.1137

Kojima, S., Tsukada, K., Otoh, S., Yamakita, S., Dymovich, A. D., & Eichwald, L. P. (2008). Geological relationship between Anyui metamorphic complex and Samarka terrane, Far East Russia. *Island Arc, 17*, 502–516.

Lallemand, S., Heuret, A., & Boutelier, D. (2005). On the relationship between slab dip, back-arc stress, upper plate absolute motion, and crustal nature in subduction zones. *Geochemistry,*

Geophysics, Geosystems, 6, Q09006. https://doi.org/10.1029/2015GC000917

Lee, G. H., & Kim, B. (2002). Infill history of the Ulleung Basin, East Sea (Sea of Japan) and implications on source rock and hydrocarbons. *Marine and Petroleum Geology, 19*, 829–845.

Lee, G. H., Yoon, Y., Nam, B. H., Lim, H., Kim, Y. S., Kim, H. J., & Lee, K. (2011). Structural evolution of the southwestern margin of the Ulleung Basin, East Sea (Japan Sea) and tectonic implications. *Tectonophysics, 502*, 293–307.

Lü, Y., Li, J., Liu, L., & Zhao, L. F. (2019). Complex uppermost mantle structure and deformation beneath the northwest Pacific region. *Journal of Geophysical Research, 124*, 6866–6879. https://doi.org/10.1029/2019JB017356

Morishita, T., Hirano, N., Sumino, H., Sato, H., Shibata, T., Yoshikawa, M., Arai, S., Nauchi, R., & Tamaru, A. (2020). Alkali basalt from the Seifu Seamount in the Sea of Japan: Post-spreading magmatism in a back-arc setting. *Solid Earth, 11*, 23–36. https://doi.org/10.5194/se-11-23-2020

Nishimura, T., & Takada, Y. (2017). San-in shear zone in southwest Japan, revealed by GNSS observations. *Earth, Planets and Space, 69*, 85. https://doi.org/10.1186/s40623-017-0673-8

Obara, K., Kasahara, K., Hori, S., & Okada, Y. (2005). A densely distributed high-sensitivity seismograph network in Japan: Hi-net by National Research Institute for Earth Science and Disaster Prevention. *Review of Scientific Instruments, 76*, 021301. https://doi.org/10.1063/1.1854197

Okada, Y., Kasahara, K., Hori, S., Obara, K., Sekiguchi, S., Fujiwara, H., & Yamamoto, A. (2004). Recent progress of seismic observation networks in Japan - Hi-net, F-net, K-net and KiK-net. *Earth, Planets and Space, 56*, 15–28.

Park, Y., Ree, J. H., & Yoo, S. H. (2006). Fault slip analysis of Quaternary faults in southeastern Korea. *Gondwana Research, 9*, 118–125.

Petit, C., & Fournier, M. (2005). Present-day velocity and stress fields of the Amurian Plate from thin-shell finite-difference modelling. *Geophysical Journal International, 160*, 357–369.

Rhie, J., & Kim, S. (2010). Regional moment tensor determination in the southern Korean Peninsula. *Geosciences Journal, 14*, 329–333. https://doi.org/10.1007/s12303-010-0038-9

Sheen, D. H. (2015). Comparison of local magnitude scales in South Korea. *Journal of the Geological Society of Korea, 51*, 415–424.

Sheen, D. H., Kang, T. S., & Rhie, J. K. (2018). A local magnitude scale for South Korea. *Bulletin of the Seismological Society of America, 108*, 2748–1755.

Sibuet, J. C., Hsu, S. K., Le Pichon, X., & Reed, J. P. (2002). East Asia plate tectonics since 15 Ma: Constraints from the Taiwan region. *Tectonophysics, 344*, 103–134.

Soh, I., Chang, C., Lee, J., Hong, T. K., & Park, E. S. (2018). Tectonic stress orientations and magnitudes, and friction of faults, deduced from earthquake focal mechanism inversions over the Korean Peninsula. *Geophysical Journal International, 213*, 1360–1373. https://doi.org/10.1093/gji/ggy061

Taira, A. (2001). Tectonic evolution of the Japanese Island arc system. *Annual Review of Earth and Planetary Sciences, 29*, 109–134.

Takahashi, Y., Cho, D. L., Mao, J., & Yi, K. (2018). SHRIMP U-Pb zircon ages of the Hida metamorphic and plutonic rocks, Japan: Implications for late Paleozoic to Mesozoic tectonics around the Korean Peninsula. *Island Arc, 27*, e12220. https://doi.org/10.1111/iar.12220

Vaes, B., van Hinsbergen, D. J. J., & Boschnan, L. M. (2019). Reconstruction of subduction and back-arc spreading in the NW Pacific and Aleutian Basin: Clues to causes of Cretaceous and Eocene plate reorganizations. *Tectonics, 38*, 1367–1413.

van Horne, A., Sato, H., & Ishiyama, T. (2017). Evolution of the Sea of Japan and some unsolved issues. *Tectonophysics, 710–711*, 6–20.

Xu, Z., Wang, S., & Huang, & Y., Gao, A. (1992). Tectonic stress of China inferred from a large number of earthquakes. *Journal of Geophysical Research, 97*, 11867–11877.

Yoon, S. H., & Chough, S. K. (1995). Regional strike-slip in the eastern continental margin of Korea and its tectonic implications for the evolution of Ulleung Basin, East Sea (Japan Sea). *Geological Society of America Bulletin, 107*, 83–97.

Zhao, D., Wang, J., Huang, Z., & Liu, X. (2021). Seismic structure and subduction dynamics of the western Japan Arc. *Tectonophysics, 802*, 228743. https://doi.org/10.1016/j.tecto.2021.228743

Zheng, Y., Shen, W., Zhou, L., Yang, Y., Xie, Z., & Ritzwoller, M. H. (2011). Crust and uppermost mantle beneath the North China Craton, northeast China, and the Sea of Japan from ambient noise tomography. *Journal of Geophysical Research, 116*, B12312. https://doi.org/10.1029/2011JB008637